The Effect of Temperature and Extrusion Speed on The Consolidation of Zirconium-Based Metallic Glass Powder Using Equal-Channel Angular Extrusion

I. KARAMAN, J. ROBERTSON, J.-T. IM, S.N. MATHAUDHU, Z.P. LUO, and K.T. HARTWIG

In this study, gas-atomized amorphous $Zr_{58.5}Nb_{2.8}Cu_{15.6}Ni_{12.8}Al_{10.3}$ (Vitreloy 106a) containing 1280 ppmw oxygen was consolidated by equal-channel angular extrusion (ECAE). The powder was vacuum encapsulated in copper cans and subjected to one extrusion pass in the temperature region above the glass transition temperature (T_g) and below the crystallization temperature (T_x). The effects of extrusion temperature and the extrusion rate on microstructure, thermal stability, hardness, and compressive strength are investigated. Compression fracture surfaces were examined to determine the deformation mechanisms. The consolidates in which the time-temperature-transformation (TTT) boundary was not crossed during processing exhibit differential scanning calorimetry (DSC) patterns similar to the initial powder, with a slight decrease in T_x. Compressive strengths of about 1.6 GPa are recorded in the consolidates processed at 30 °C and 40 °C below T_x, which is close to what is observed in cast counterparts. The fracture surfaces exhibit vein patterns covering up to 90 pct of the surface area in some samples, which are characteristic of glassy material fracture. The slight decrease in T_x after consolidation is attributed to thermal-history-dependent short-range order and formation of nanocrystalline islands. The present results show that ECAE is successful in consolidation of metallic glass powder. This processing avenue opens a new opportunity to fabricate bulk metallic glasses (BMGs) with dimensions that may be impossible to achieve by casting methods.

I. INTRODUCTION

OVER the last two decades, the science and engineering of metallic glasses has progressed rapidly. The promising characteristics of this class of materials include high tensile strength, hardness, corrosion resistance, and impact fracture energy, as well as viscous deformability.[1,2] Metallic glasses are appealing materials for applications in many commercial industries, including medicine, sports, telecommunications, and machining.[2] It has also been shown that metallic glasses fail by shear localization during ballistic impact conditions, making them appealing for kinetic-energy-penetrator applications.[3]

Considerable efforts have been made to produce bulk metallic glasses (BMGs). In the past, it was only possible to produce metallic glasses as thin ribbons due to the rapid cooling rates necessary to achieve an amorphous state. In the last decade however advances in the selection of compositions of glass-forming alloys have made it possible to produce cast bulk materials. Some Zr- and Cu-based alloys can achieve vitrification with cooling rates as low as 1 K/s.[1] However, the dimensions achievable with casting methods are still considerably smaller than what is required for some structural applications, where the use of BMGs is appealing.

One technique for the fabrication of bulk glasses is powder consolidation. The potential of consolidation lies in the fact that this method does not require a substantial thickness of amorphous metal to cool rapidly from the melt. There are two methods that have been used to consolidate metallic glass powder: hot pressing and conventional area-reduction extrusion. In the case of hot pressing, it is difficult to achieve full density on large dimensions.[4,5] Conventional extrusion, on the other hand, has shown promise for fabricating bulk material that is near-full density, has good particle-to-particle bonding, and exhibits tensile strengths comparable to cast amorphous material.[4,5,6] However, the area reduction required to achieve sufficient bonding between particles may be a limiting factor for conventional extrusion consolidation.

As an alternative method of powder consolidation, the authors have recently utilized equal-channel angular extrusion (ECAE) to consolidate Cu-based metallic glass powders in the supercooled liquid region.[7] The ECAE method subjects a volume of material to simple shear deformation by forcing it through two intersecting channels. This has some advantages over conventional extrusion: the workpiece experiences nearly uniform strain, the cross section of the workpiece remains constant, and ECAE can be accomplished at low extrusion loads. These advantages make it theoretically possible to fabricate large-cross-sectional amorphous materials. It has already been shown that ECAE is effective in powder consolidation.[7,8,9] Full theoretical density from 6061 Al powder is achieved after, at most, two extrusions through a 90-deg tool. The tensile strength of the ECAE consolidated aluminum is comparable to that of wrought material.[8] Other materials successfully consolidated using ECAE have included Cu blended with Ag, Sn-8Cu blended with Al_2O_3 and SiO_2, NbFeB blended with 304 stainless steel or pure Cu, WC blended with Co, and amorphous Cu-based alloys.[7,8,9,10,11] Consolidation of $Cu_{50}Ti_{32}Zr_{12}Ni_5Si_1$ (Vitreloy 102) metallic glass powders with ECAE resulted in bulk samples with an

I. KARAMAN, Assistant Professor, J. ROBERTSON, J.-T. IM, and S.N. MATHAUDHU, Graduate Research Assistants, and K.T. HARTWIG, Professor, Department of Mechanical Engineering, and Z.P. LUO, Research Scientist, Microscopy and Imaging Center, are with Texas A&M University, College Station, TX 77843. Contact e-mail: thartwig@mengr.tanu.edu

Manuscript submitted December 30, 2002.

amorphous character and a supercooled liquid region slightly narrower than that of the initial powder.[7] The change in the supercooled liquid region, as well as the increase in hardness and brittleness after consolidation, was attributed to the high oxygen content of the initial powder (>2000 ppmw) and to crossing the time-temperature-transformation (TTT), or crystallization, boundary during processing, leading to partial devitrification.

The aim of the present study is to consolidate a high-pressure gas-atomized (HPGA) zirconium-based metallic glass powder, characterize the physical and mechanical properties of the consolidate, and compare the properties of the consolidate with that of the initial powder and cast counterparts. Special care was taken during processing so that the consolidating powder would not cross the TTT boundary during ECAE.

II. EXPERIMENTAL PROCEDURE

The starting powder was made at the Materials Processing Center of the United States Department of Energy–Ames Laboratory (Ames, IA) by high-pressure gas atomization. The atomization used a 4 kg charge of Vitreloy 106a, with a composition of Zr-15.6Cu-12.8Ni-10.3Al-2.8Nb (in at. pct). The initial charge was obtained by induction skull casting and contained approximately 950 ppmw oxygen and 100 ppmw carbon. The ingot was melted in a graphite crucible in an argon atmosphere (<250 ppmw O_2), poured into the atomizer at 1350 °C, and atomized with He gas. Inert-gas-fusion analysis of the resulting powder sieved to 75 μm showed 1280 ppmw oxygen and 226 ppmw carbon, respectively.

The morphology of the HPGA V106a powder is shown in Figure 1. For the ECAE consolidation experiments, the powder (38 μm < diameter < 150 μm) was placed uncompacted into copper cans, vacuum outgassed for 8 hours at 150 °C, and sealed using electron-beam welding. The dimensions of all ECAE containers were 19 × 19 × 90 mm. The powder chamber was 13 mm in diameter and 50-mm long. Figure 2 illustrates a schematic of powder in a can before and after consolidation, as well as an image of the consolidated V106a in a Cu can.

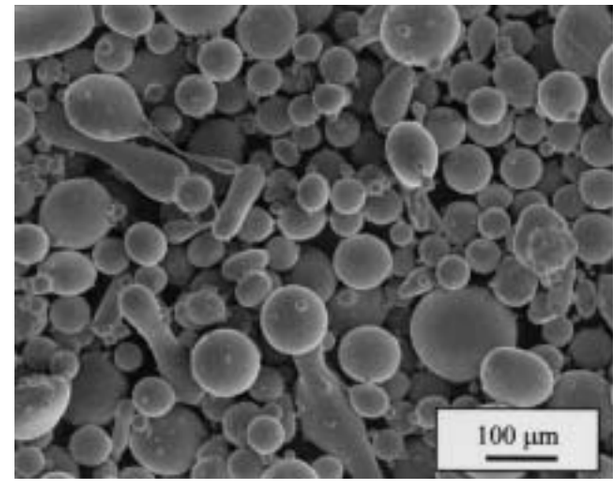

Fig. 1—Spherical and platelike morphology of high pressure gas atomized V106a powder.

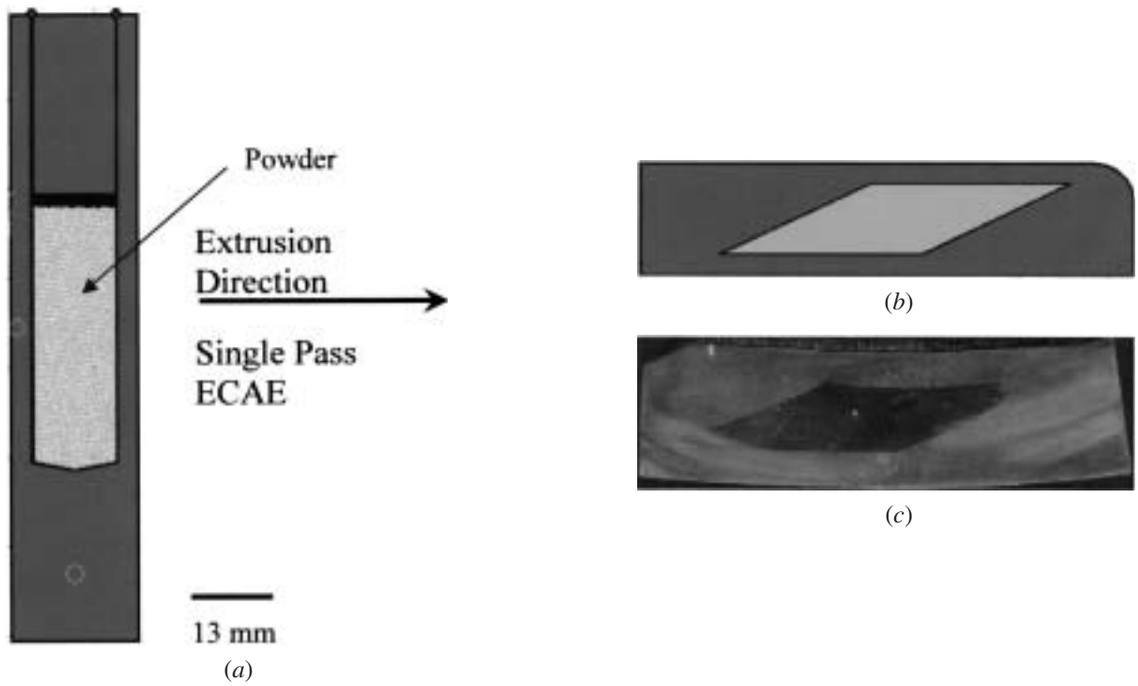

Fig. 2—A schematic of an ECAE can filled with Vitreloy 106a powder: (*a*) illustration before extrusion, (*b*) illustration after one pass ECAE, and (*c*) actual consolidated Vitreloy 106a in the Cu can.

Prior to ECAE, the die assembly was heated to a set temperature. Room-temperature cans were then dropped into the die and allowed to heat to the die temperature. The temperature of the can immediately prior to extrusion was monitored by thermocouples: one was located on the backside of the can in the center of its length; the other was placed in the center of the can 10 mm from the bottom. The heating rate in the can was higher than 60 K/min up to T_g. Seven single-pass extrusions were performed at varying temperatures and extrusion rates, as described in Table I.

To select proper extrusion parameters (extrusion rate and time) at a given temperature so that crystallization would not occur, a TTT diagram was determined for the V106a powder (Figure 3). This diagram was created by performing isothermal differential scanning calorimetery (DSC) runs on the powder at varying temperatures across the supercooled liquid region. This was accomplished by heating the powder at a rate of 40 K/min to an annealing temperature above T_g, and then measuring the time until the first exothermic peak, which indicates the onset of crystallization. A DSC run on the initial powder at 40 K/min gives T_g and T_x values of 398 °C and 460 °C, respectively, as shown in Table I.

Light microscopy was used to examine the microstructure of the consolidated materials. The samples were etched for 3 seconds at 298 K in a solution of 10 vol pct hydrofluoric acid and 90 vol pct distilled water. The oxygen content of the consolidates was measured using a LECO* TC-436 01N analyzer. The density of the consolidated samples was determined using the buoyancy method, applying the Archimedes principle. The values of T_g and T_x were determined by performing DSC scans at a rate of 40 K/min with a Perkin Elmer (Wellesley, MA) Pyris I apparatus. Vickers microhardness measurements of the powder and the consolidates were taken using loads of 100 and 500 g, respectively. The X-ray diffraction (XRD) technique was used to examine the amorphous character of the consolidates utilizing a Bruker-AXS D8 diffractometer with Cu K_α radiation. Microhardness measurements were also carried out along the length of the flow plane (*i.e.,* side plane of the billet parallel to the extrusion direction) of samples Cu050, Cu052, and Cu053. Compression samples of consolidated V106a were electrodischarge machined (EDM) to a 3-mm diameter and 6-mm length. The compression tests were conducted using an MTS testing machine at room temperature and at a strain rate of 10^{-4}. The strain was measured using a miniature extensometer. The fracture-surface appearance was examined using a JEOL* JSM-6400 scanning electron microscope. The microstructures of selected consolidates were investigated utilizing transmission electron microscopy (TEM). The TEM foils were prepared from bulk samples by mechanical thinning slices to 100 μm, punching 3 mm disks, and ion milling. A JEOL 2010 microscope operated at a nominal accelerating voltage of 200 kV was used.

*LECO is a trademark of the LECO Corporation, St. Joseph, MI.

*JEOL is a trademark of Japan Electron Optics Ltd., Tokyo.

III. RESULTS AND DISCUSSION

The consolidation experiments were conducted at four different temperatures (T_g, T_g + 20 °C, T_g + 30 °C, and T_g + 40 °C) to evaluate the effect of temperature on the resulting consolidates. Strain-rate effects were studied at T_g + 20 °C using three different extrusion speeds (1, 6, and 12 mm/s). The measured temperature rise during extrusion due to deformation heating and friction was significant in some cases. The maximum rise in temperature was about 30 °C at the front part of the billet, in the experiments

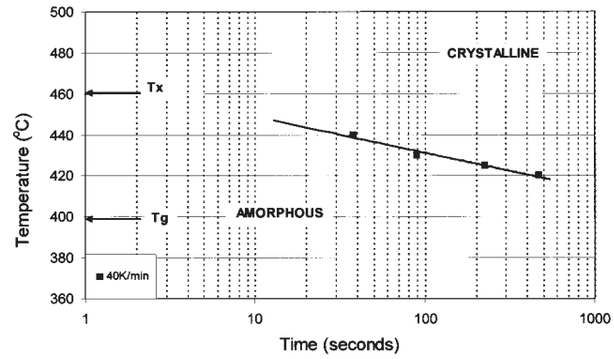

Fig. 3—TTT diagram for the onset of crystallization of metallic glass powder heated to selected temperatures at 40 K/min.

Table I. Summary of V106a Powder Extrusion Consolidation Parameters Used for ECAE and Some of the Resulting Properties Including Aspect Ratio of Sheared Powder, Glass Transition Temperature (T_g), Crystallization Temperature (T_x), Range of the Supercooled Region (ΔT), Microhardness value, and Enthalpy of Crystallization for All Consolidates and the Initial Powder (BT Represents a Broken Thermocouple during Extrusion)

Experiment ID	Cu050	Cu051	Cu052	Cu053	Cu054	Cu058	Cu059	Powder
Die set temp (°C)	440	420	420	420	400	430	430	—
Extrusion speed (mm/s)	6	1	6	12	6	6	6	—
Aspect ratio	5.6 ± 0.3	4.2 ± 0.6	4.4 ± 0.3	6.2 ± 1.1	3.6 ± 0.8	4.1 ± 0.4	1.8 ± 0.3	1.2 ± 0.3
ΔT (°C)	37	50	58	53	60	58	57	62
T_g (°C)	402	405	398	400	399	400	400	398
T_x (°C)	439	455	456	453	459	458	457	460
Time above T_g (s)	263	200	BT	BT	23	270	BT	NA
Hardness (Hv 500 g)	504 ± 6	470 ± 5	472 ± 17	487 ± 6	470 ± 11	469 ± 17	485 ± 5	467 ± 35
Density (g/cm^3)	6.6	NA	6.27	NA	NA	6.39	NA	NA
Enthalpy of crystallization (ΔH) (J/g)	2.2	24.8	24.3	21.6	28.6	23.8	25.3	31.2

where temperature measurements were successful. In these experiments, the time that the samples were exposed to temperatures above T_g was shorter than what is required for the start of significant primary crystallization.

A. *Effect of Extrusion Temperature on The Consolidate Properties*

Figure 4 shows the microstructure on the flow plane of etched samples that were consolidated at 400 °C, 420 °C, 430 °C, or 440 °C with an extrusion speed of 6 mm/s. Except for sample Cu054, which was processed at T_g, all of the samples (processed at T_g + 20 °C, T_g + 30 °C, and T_g + 40 °C) demonstrate good consolidation without any significant porosity, judging from the optical microscopy images. The density measurements (Table I) show that the density of the consolidates increases with increasing consolidation temperature. The density of the initial powder and cast V106a is not known; however, the density of V106 is 6.8 g/cm^3.[12] Since the Nb content in V106a is half that of V106 (5 at. pct), the density of V106a should be slightly lower than 6.8 g/cm^3; 6.7 g/cm^3 is a good estimate. Therefore, the Cu052, Cu054, and Cu050 samples in Table I may not have full density.

It is apparent from the elongated shape of the particles that significant shear deformation occurs during extrusion. The deformed aspect ratio of prior particles is near the theoretical value (~5) that is expected from ECAE deformation of a spherical perfectly plastic particle. The aspect ratios of the deformed particles are also tabulated in Table I. Sharp triple junctions are evident in Figures 4(b) through (d), verifying easy flow and good consolidation. The sample consolidated at 400 °C exhibits significant porosity and relatively poor consolidation. The lack of sufficient deformation and, thus, lack of good consolidation is attributed to the increase in viscosity at the lower temperature. As compared to previous consolidation efforts on Cu-based metallic glass powder by ECAE,[7] the present Zr-based metallic glass powder exhibits more deformation after a single-pass extrusion. This is probably because of the better temperature control during ECAE, lower oxygen content of the initial material, and lower viscosity during shear.

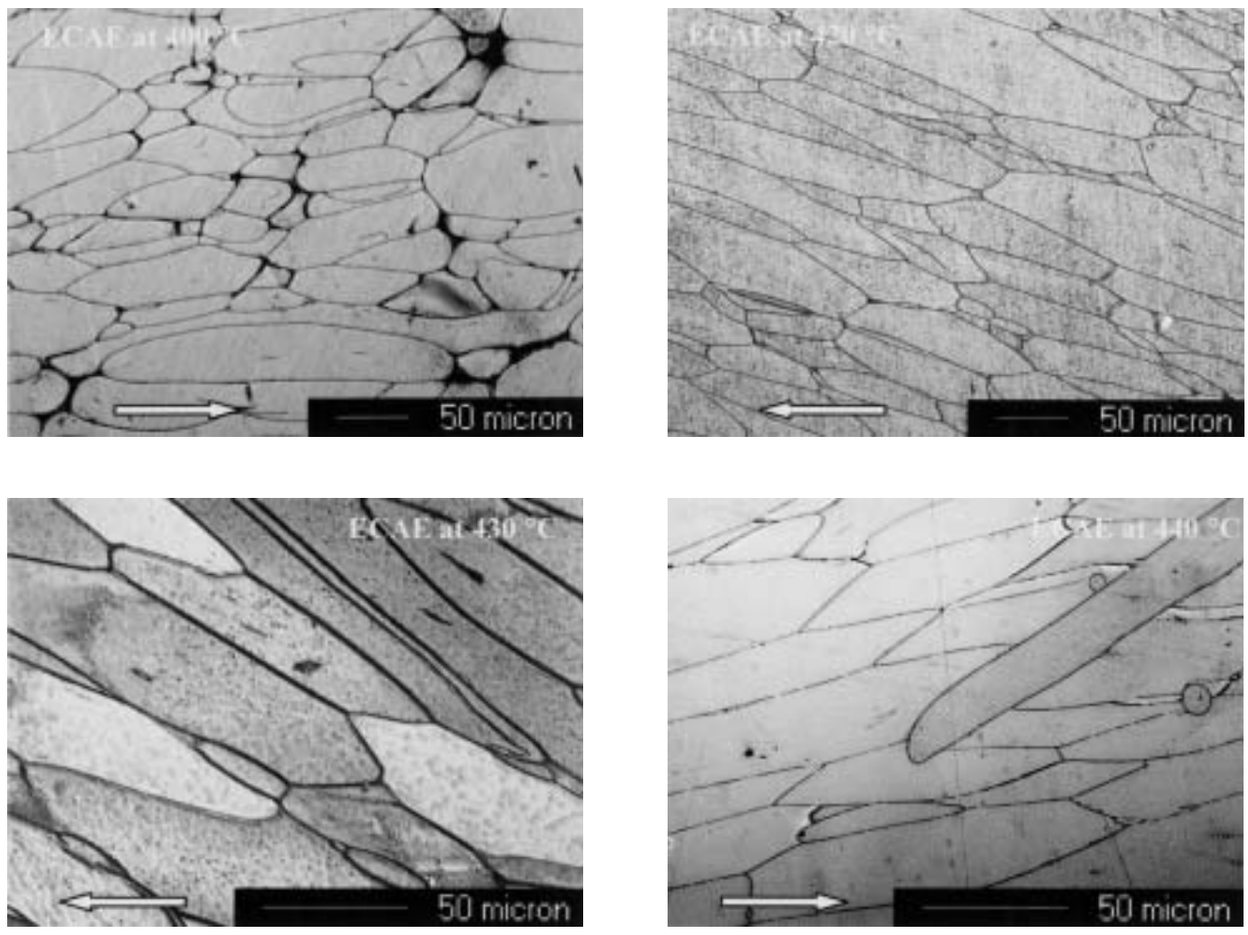

Fig. 4—Optical micrographs of the flow plane of the (*a*) Cu054, (*b*) Cu052, (*c*) Cu058, and (*d*) Cu050 etched samples showing how the morphology of prior particles and porosity content of the consolidates change with increasing extrusion temperature. Refer to Table I for extrusion conditions. The extrusion direction is shown by an arrow in each micrograph.

The oxygen content of the consolidates was measured to check whether there was an increase in oxygen during the canning or processing steps. Except for Cu054, which was consolidated at T_g, all consolidates had similar oxygen contents to the initial powder. The higher oxygen content in Cu054 is attributed to inadequate electron-beam welding of the can. Therefore, another reason why the consolidation is poor in Cu054 (Figure 4(a)) may be because of a higher oxygen content, which can cause an increase in viscosity.

A typical polished and unetched sample consolidated at 420 °C is presented in Figure 5(a), illustrating a small amount of porosity. After etching the sample on the transverse plane (*i.e.,* front plane of the billet, perpendicular to the extrusion direction), the prior particle boundaries can be seen (Figure 5(b)), clearly showing severe deformation of a platelike prior particle forming sharp triple junctions and apparently good bonding with neighboring particles. This demonstrates that this combination of temperature (T_g + 20 °C), extrusion speed (6 mm/s), and hydrostatic pressure (caused by the copper cans) is sufficient to cause flow for good bonding. Good bonding is substantiated by the compressive strength of the samples described subsequently.

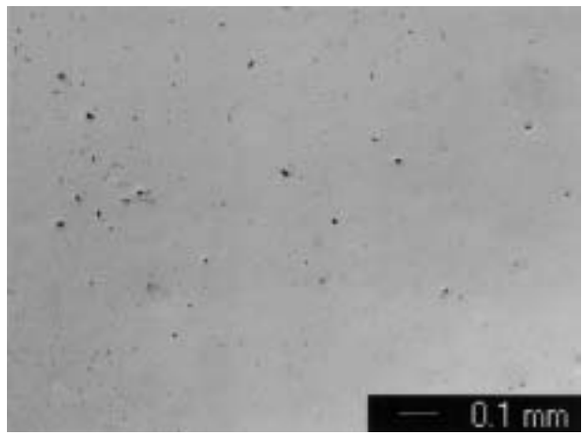

(*a*)

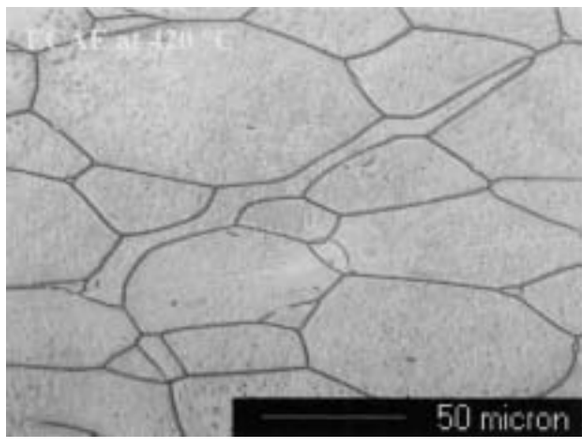

(*b*)

Fig. 5—Optical micrograph of (*a*) unetched and (*b*) etched transverse plane (the extrusion direction is perpendicular to the plane of the paper) of the Cu052 consolidate.

The observation of etched prior particle boundaries in all consolidates is unexpected, as the fully amorphous structure should not reveal any boundaries. This observation is attributed to the surface oxide layer on the as-received powder. The TEM investigations did, indeed, demonstrate that some of these prior particle boundaries are decorated with yttrium oxide particles, as shown in Figure 6. However, these particles do not form a continuous boundary at the prior particle boundaries. Y_2O_3 originates from the HPGA process, where it is used as a sealant in the crucible orifice channel.

The DSC scans for the 400 °C, 420 °C, 430 °C, and 440 °C consolidates are presented in Figure 7 together with that of the initial powder. The T_g and T_x values for each curve are obtained by finding the points where the slope changes on the first endothermic and exothermic peaks, respectively. The values of T_g, T_x, ΔT, and the enthalpy of crystallization (ΔH) for each heat-flow curve are summarized in Table I. The T_g values for the powder and for all of the consolidates are approximately the same. The DSC scans of the powder consolidated at 400 °C, 420 °C, and 430 °C show a slight decrease in T_x (and, thus, ΔT) compared to that of the powder, as well as a slight decrease in the enthalpy of primary

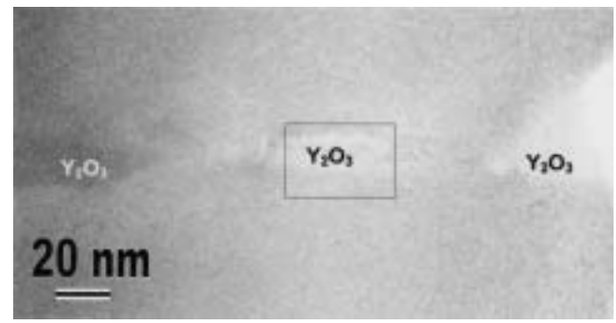

Fig. 6—High-resolution TEM image of prior particle boundary in the V106a powder consolidate processed at 420 °C with 6 mm/s extrusion speed. The crystalline region is found to be Y_2O_3. A continuous crystalline layer is not found along the prior particle boundaries which can be an indication for the effectiveness of ECAE to distrupt the oxide layer that coats all gas-atomized V106a particles. The oxide particles are what cause the etched boundaries in the light microscopy images.

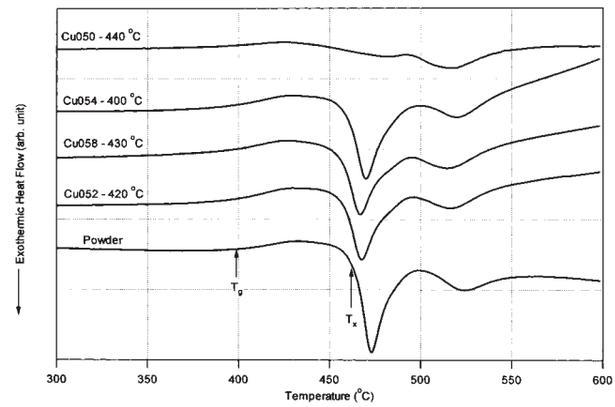

Fig. 7—Continuous DSC curves for each of the characterized V106a consolidates and the starting powder showing the effect of extrusion temperature on the characteristic temperatures. The heating rate is 40 K/min.

crystallization. There is an apparent trend in the extrusion-temperature dependence of the primary crystallization-peak location. The peak is shifted to lower temperatures with increasing extrusion temperature. The significant drop in the primary crystallization peak on the DSC scan for Cu050, extruded at 440 °C, indicates that devitrification occurred during extrusion.

Figure 8 presents XRD patterns from the starting powder and the consolidates. There is no significant evidence of crystallization, except for samples Cu050 and Cu053. The Cu050 sample shows relatively strong crystalline peaks which are consistent with the DSC scans that indicate the occurrence of primary crystallization. The peak position in the Cu050 sample is also shifted to the right-hand side, showing crystallization. Although the decrease in the enthalpy of primary crystallization (Table I) in some of the consolidates (*i.e.,* Cu058) and TEM images (Figure 13, Cu058) is indicative of some nanocrystallization, it was not clearly evident in the XRD pattern. This is because the ability of the X-ray diffractometer is rather limited when very small crystalline regions are present.[4]

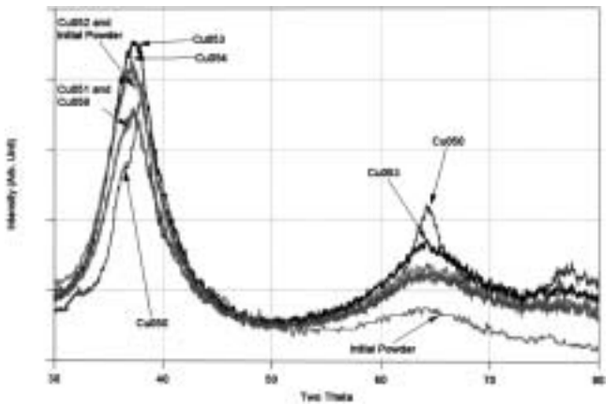

Fig. 8—X-ray diffraction patterns of selected ECAE consolidates.

Vickers microhardness measurements were taken on polished unetched surfaces of the powder and consolidates. The results from the microhardness measurements are listed in Table I. Microhardness indentations on the powder show shear banding around the indentation, attesting to its amorphous character (Figure 9(a)). Hardness measurements under a 500-g load (Figures 9(b), (d), and (f)), taken on consolidates without significant porosity, *i.e.,* Cu050, Cu052, and Cu058, also exhibit shear banding around indentations, indicative of an amorphous phase. When the load is increased to 1 kg, Cu050, processed at 440 °C, exhibits significant cracking around the indentation, attesting to a relatively brittle character (Figure 9(f)), and this is in correlation with the DSC results. The lower-temperature consolidates do not experience any sign of brittle fracture (Figure 9(c)). The Cu054 consolidate processed at 400 °C shows shear banding but also displays cracking. The hardness values in Table I are correlated with the microstructural observations: the higher the extrusion temperature, the higher the hardness value. This trend is similar to the change in T_x with an increase in extrusion temperature and can be attributed to the microstructural changes that occur during consolidation at different temperatures.

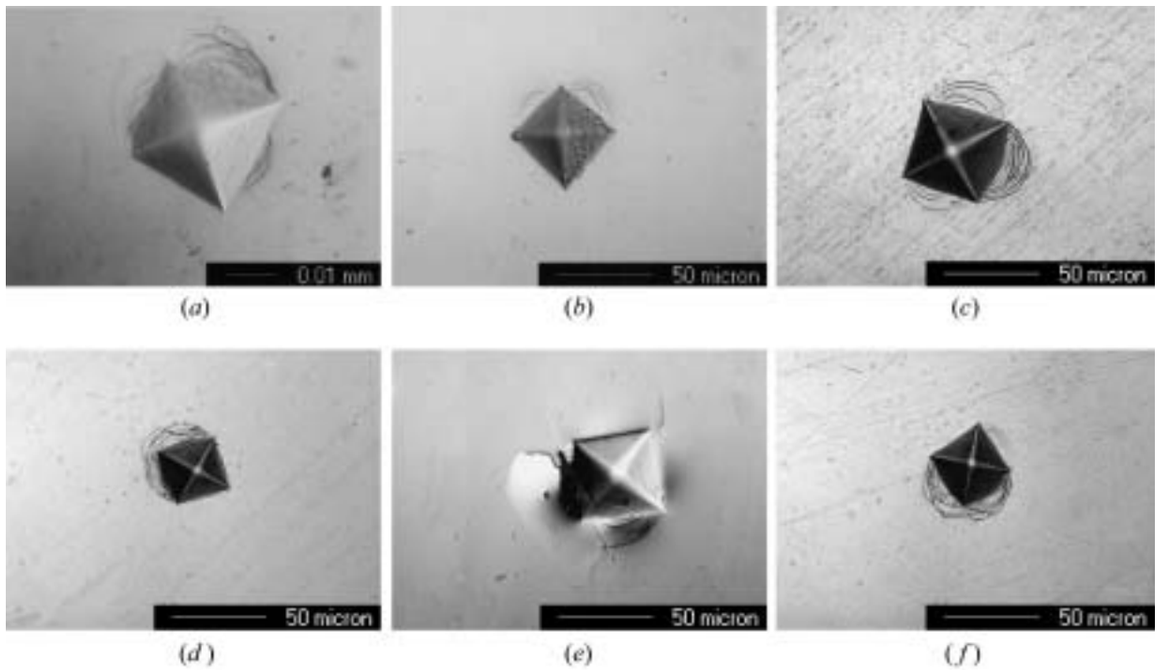

Fig. 9—Vickers microhardness indentations on (*a*) starting glassy powder under 200 g, (*b*) sample Cu052 under 500 g, (*c*) Cu052 under 1 kg, (*d*) Cu050 under 500 g, (*e*) Cu050 under 1 kg, and (*f*) Cu058 under 500 g. Shear bands radiating from the indents without any cracking are an indication of amorphous character. The cracking in (e) demonstrates embrittlement.

The results of compression experiments on consolidated V106a are presented in Figure 10. The experiments were conducted on three different regions of the consolidate: the front, middle, and back along the extrusion direction. For comparison purposes, the compressive stress-strain response of cast V106[13] is included in the figure (data on the cast V106a are not available). It is apparent that the Cu050, Cu052, and Cu058 consolidates demonstrate compressive strengths close to that of cast material, verifying good consolidation. The ultimate compressive strength of the V106a test specimens is between 1400 and 1700 MPa, compared to a compressive strength of 1780 MPa for the cast V106. The failure strain is between 2 and 3 pct for both the consolidated and cast materials.

Serrated flow, observed especially in Cu052, is an indication of shear banding, which is expected in metallic glasses. The development of serrated flow and the slight increase in work hardening associated with the serrated flow are, presumably, because shear bands generate along the whole outer surface of the samples and the massive movement of the atoms in the shear bands is suppressed by the crossing of different shear bands. The lower load level in the case of the Cu052 front-region sample is because of inferior consolidation near the copper can–metallic glass powder interface. Poor consolidation and occasional small cracks were common at the interface for the low-temperature consolidate.

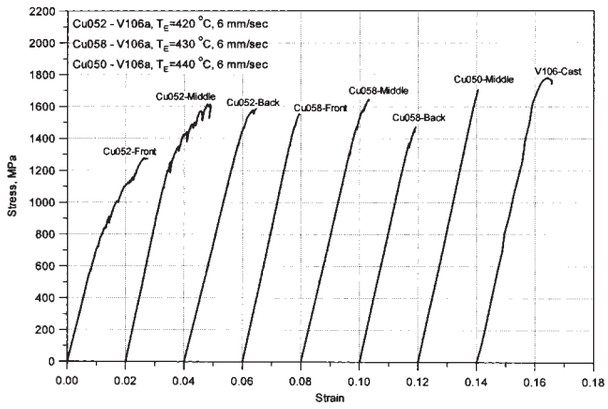

Fig. 10—Compression experiments on the ECAE consolidated V106a samples and cast V106. The test specimens were 3 mm in diameter by 6 mm in length. The strain rate was 10^{-4}.

The compressive fracture surfaces are investigated using scanning electron microscopy, as shown in Figure 11. All of the compression samples shown in Figure 10 exhibit adiabatic shear banding on a 45 deg plane to the compressive load direction, and the fracture surface consists of well-developed vein patterns (Figure 11(a)), a typical fracture characteristic of metallic glasses with good ductility.[14] The diameter of the veins is 2 to 8 μm, which is slightly higher than what is usually observed in cast samples (1 to 2 μm) and is about 10 to 40 times larger than that for melt-spun ribbons deformed at room temperature (0.2 μm).[13] The increase in the width of the veins may be related to the temperature increase during the final adiabatic fracture, because of the suppression of final fracture and good local ductility. This also implies an increase in the thickness of the shear-deformation region.

Once shear bands form, probably at surface stress-concentration points, they propagate through the sample along a 45-deg plane, and once they reach a weak spot of consolidation, interparticle debonding starts (Figure 11(b)). Larger shear steps caused by shear sliding are also evident, as observed in Figure 11(b). Interparticle debonding, in the present case, usually occurs on planes oriented in the extrusion direction. This behavior was observed previously when there was insufficient bonding between Al6061 particles consolidated using ECAE.[8] For the current study, in all cases, more than 50 pct of the fracture surface consists of vein patterns. There was no evidence of brittle fracture in these samples. The weak consolidation spots, indicating nonuniformities in consolidation, are attributed to the lack of sufficient shear or hydrostatic pressure combined with shear.

Although the compressive stress-strain response of the consolidates (Cu052 and Cu058) and the corresponding fracture-surface appearances demonstrate the amorphous character of the consolidates, the shift in the primary crystallization peak in the DSC scans, the slight decrease in ΔT, and the enthalpy of primary crystallization as compared to that of the initial powder may imply either the formation of short-range order or the formation of nanocrystalline islands caused by partial devitrification. This hypothesis excludes the possibility of the formation of large crystalline grains, as they

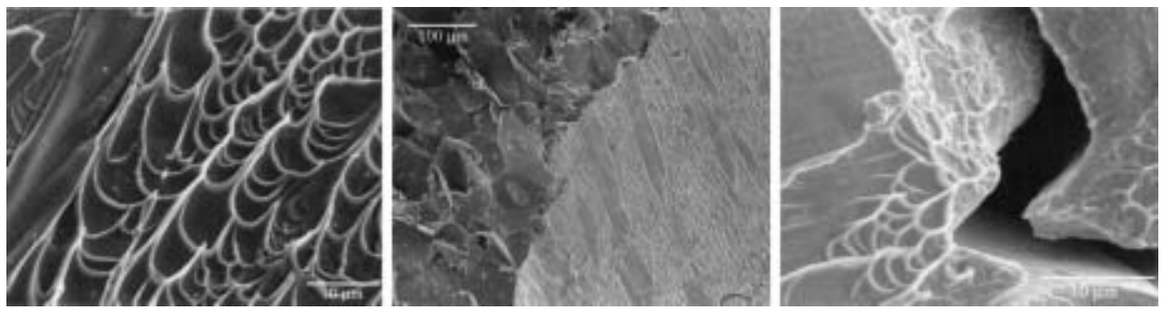

(*a*) (*b*) (*c*)

Fig. 11—SEM of the fracture surfaces of V106a compression samples: (*a*) and (*b*) from Cu058 and (*c*) from Cu052. Shear bands with well-developed vein patterns, shear slipped regions and interparticle debonding.

would cause brittle fracture, hinder shear banding and the formation of vein patterns, and exhibit low compressive strength. However, the samples tested did not show the type of brittle fracture that large crystalline phases would cause.

Considering the fact that all samples had weak interparticle-bonding spots and, therefore, debonding occurred, three remedies can be recommended to improve the interparticle bonding. First, instead of Cu, Ni cans can be used to increase the hydrostatic pressure. It is believed that increased hydrostatic pressure will help shear-deformation consolidation. Second, multipass extrusions can improve the interparticle bonding as the shear-deformation level increases. For this, more time before crystallization, *i.e.,* a larger temperature-processing window, is needed; thus, the powder should have a lower oxygen content than the present one. Last, the lower oxygen content would also assure that the viscosity is lower, leading to better flow and, thus, better bonding. These remedies are currently being implemented.

A rationale for changes observed in the DSC scans of the consolidates is that it was caused by differences in thermal history between the gas-atomized powder and the consolidate.[4] During consolidation, the powder heats to a temperature above T_g, is held there during consolidation, and then cools down. It is likely that this causes short-range ordering or the formation of nanocrystalline islands that, upon reheating, can act as nuclei for crystallization. Thus, crystallization can start at a lower temperature during successive DSC runs.

To test the effect of thermal history or annealing on thermal characteristics of the metallic glass, isochronal annealing experiments were conducted on a cast material slightly above T_g. The duration of these experiments was shorter than what is required for the start of clear crystallization (TTT boundary definition). Since V106a cast samples were not available, cast V105 samples ($Zr_{52.5}Cu_{17.9}Ni_{14.6}Al_{10}Ti_5$) were used to demonstrate the concept. The V105 cast material has a T_g = 400 °C and a T_x = 465 °C. These experiments were performed using DSC by ramping the sample up to a holding temperature at 40 K/min, holding the specimen at the specified temperature for 30 seconds, cooling it back to room temperature, and then doing a final classical DSC run at 40 K/min. Figure 12 exhibits the DSC scans of the initial sample together with ones from the annealed samples. It is clear in the figure that there is a significant shift in T_x to lower temperatures upon short annealing. The higher the annealing temperature, the lower the resulting T_x. Therefore, annealing above T_g, even if it is for a very short time, probably originates enough local motion of atoms to form short-range order, so that crystallization becomes easier upon reheating.

To investigate whether there was any nanocrystallization in the ECAE consolidates, the consolidates processed at 430 °C and 420 °C were examined using TEM. The representative structures from each are presented in Figure 13. The small black dots in Figure 13(a) (sample Cu058) are attributed to the formation of nanocrystalline islands. The existence of small peaks in the corresponding diffraction pattern supports this conclusion. However, in sample Cu052 (Figure 11(b)), no evidence of nanocrystallization is detected in both the TEM image and the electron diffraction pattern. It is likely that the length scale for short-range order is below the resolution of the TEM apparatus used.

The Cu050 sample clearly has undergone partial devitrification, as is apparent in the DSC scan (Figure 7), which shows a significant decrease in the enthalpy of primary crystallization. It could be argued that this sample should experience brittle fracture with low strength levels and a corresponding fracture-surface appearance indicative of brittle fracture because of crystallization. However, the strength level of this sample is quite high, and the fracture surface clearly demonstrates shear deformation and vein patterns similar to samples Cu052 and Cu058. Inoue[15] has recently demonstrated that Zr-based metallic glasses containing

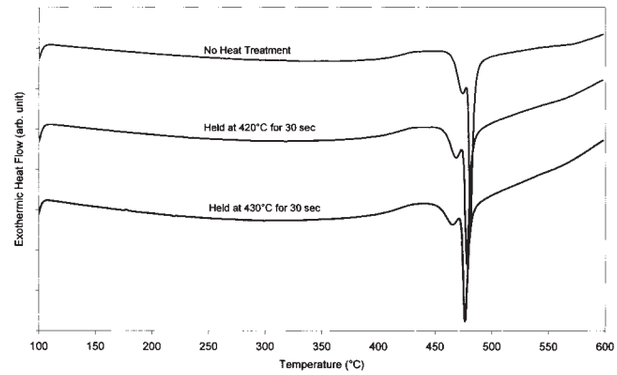

Fig. 12—DSC curves taken at 40 K/min on annealed V105 casts. The annealing heat treatment was performed by ramping to the annealing temperature at 40 K/min in the DSC and cooling rapidly back down to room temperature.

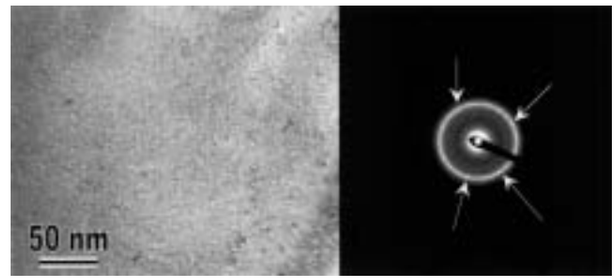

(*a*)

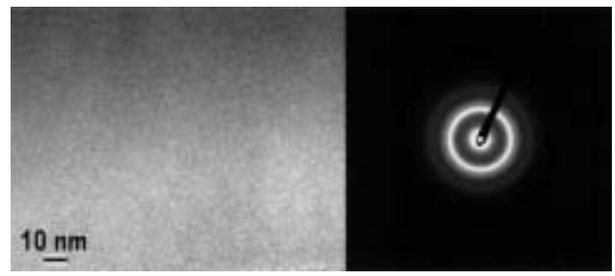

(*b*)

Fig. 13—High-resolution TEM image of the powder consolidates processed at (*a*) 430 °C and (*b*) 420 °C with 6 mm/s extrusion speed. The small black dots in (a) are believed to be nanocrystalline islands because the corresponding diffraction pattern contains sharp spots in the ring, as shown by the arrows. The sample in (b) apparently has less ordering than the sample shown in (a).

nanoscale compound particles exhibit high strength and good ductility even at volume fractions up to 20 to 30 pct, depending on the matrix and the compound. This is attributed to an amorphous matrix resistant to shear deformation, the high strength of the dispersed particles, and the highly dense packed-interface structure. Similarly, it is believed that in the present case, nanoscale crystalline islands form during consolidation. This leads to a decrease in T_x because these islands can serve as epitaxial nucleation points that grow upon heating. Moreover, the fracture still occurs along the maximum shear plane, which is inclined by about 45 deg to the direction of the load, and the fracture surface consists mainly of well-developed vein patterns. This is in agreement with Inoue's observations, in which the samples containing up to 40 pct nanoscale particles experienced a fracture mode similar to glassy single-phase alloys.[15]

B. *Effect of Extrusion Speed on The Consolidate Properties*

Two of the extrusions that were processed at 420 °C were extruded with different extrusion speeds (1 and 12 mm/s) to evaluate the effect of strain rate. Optical microscopy images of Cu053, which was extruded at 12 mm/s, show extensive deformation and elongation of the prior particles in certain regions of the consolidate (Figure 14(a)), but little deformation in other areas (Figure 12(b)). The deformation is not uniform, and the porosity content is higher than in Cu051 and Cu052, which were consolidated at the same temperature (compare Figure 14(b) with Figures 14(c) and 4(b)). The higher porosity content is attributed to the higher strain rate, which is estimated as 2.7 s^{-1}. At this strain rate, Zr-based metallic glasses experience inhomogeneous deformation which is characterized by discrete shear banding, high localized adiabatic heating, and plastically undeformed regions.[6] For a similar alloy and deformation temperature, it has been predicted[6] that the highest strain rate that will yield a homogeneous deformation is about 0.5 s^{-1} during conventional extrusion consolidation. The strain rate for sample Cu051 was 0.22 s^{-1}, at which it experienced homogeneous deformation, supporting the previous prediction. In the Cu052 sample (Figure 4(b)), the strain rate was 1.3 s^{-1} and above the predicted limit for homogeneous deformation during conventional extrusion consolidation. However, homogeneous deformation was observed in this sample, indicating that ECAE consolidation may allow homogeneous deformation under higher strain rates than what is possible for conventional extrusion consolidation.

Figure 14(c) shows an optical micrograph of the flow plane of sample Cu051, consolidated at 1 mm/s. For this case, the particles deformed more uniformly but experienced less elongation than some regions extruded at 12 mm/s and the material extruded at 6 mm/s. The decrease in elongation as compared to Cu052 and Cu053 could be due to either the higher viscosity at the lower strain rate[16,17] or the formation of a crystalline phase due to longer exposure to temperatures above T_g during extrusion. The amount of deformation depends on the temperature and strain rate, which both influence the viscosity of the material.

The DSC scans of the samples consolidated at 420 °C with different extrusion rates are presented in Figure 15. The T_g value of the consolidates does not change appreciably with the change in extrusion rate. The T_x value is lower in the consolidates as compared to that of the initial powder; however, there is not a direct relation between the decrease in T_x and the strain rate. The sample consolidated with the highest strain rate (12 mm/s) experienced the highest drop in T_x, whereas the sample consolidated with the lowest strain rate (1 mm/s) does not have the lowest decrease in T_x. This anomaly can be attributed to the exposure time to the annealing temperatures above T_g during processing. If the shift in T_x were only related to the rate of deformation and, thus, to deformation heating, then the shift in T_x would be correlated with the strain rate. It is likely that the Cu051 sample was exposed to annealing temperatures above T_g for longer times than Cu052, and more nanoscale particles formed. Similarly, although the exposure in Cu053 should have been shorter, the adiabatic heating and nonuniform deformation at high strain rates may have caused nanoscale particle formation in the matrix. The hardness measurements support this correlation that the lower the shift in T_x, the closer the hardness value is to that of the initial powder, implying less devitrification (refer to the hardness values in Table I).

In summary, the effect of strain rate on consolidation is a complicated issue. When investigating strain-rate effects, one should consider (1) how viscosity changes with strain rate at a given temperature, (2) how adiabatic heat generation during deformation changes with increasing strain rate, and (3) the strain-rate and temperature conditions below which the deformation is expected to be uniform. From the present

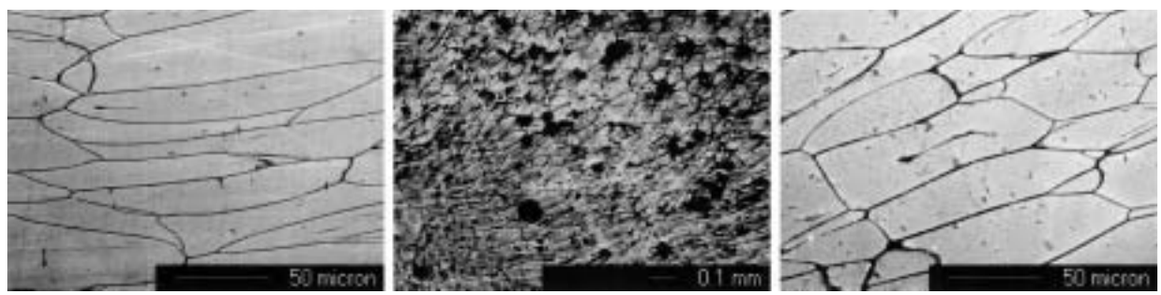

(*a*) (*b*) (*c*)

Fig. 14—Optical micrograph of the flow plane of (a), (*b*) Cu053 and (*c*) Cu051 showing how the morphology of prior particles and porosity content of consolidates change with increasing extrusion rate. Refer to Table I for extrusion conditions.

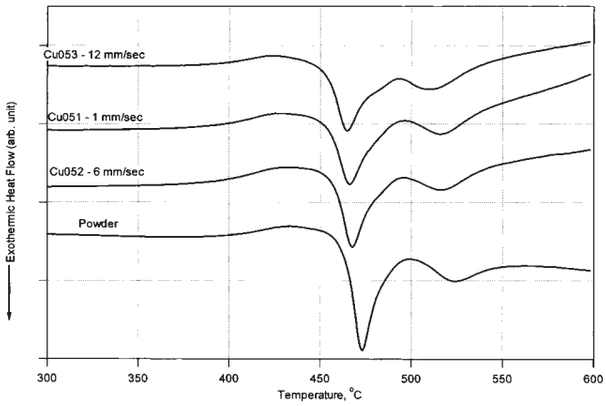

Fig. 15—Continuous DSC curves for V106a consolidates and the starting powder showing the effect of extrusion speed on the characteristic temperatures. The heating rate was 40 K/min.

experiments, it appears that an extrusion speed of 6 mm/s is found to be the best rate at 420 °C for desirable consolidate characteristics.

IV. CONCLUSIONS

Gas-atomized Vitreloy 106a powder was consolidated using ECAE in the supercooled liquid region at different strain rates and temperatures. The microstructure of all consolidates shows significant particle deformation. The increase in aspect ratio of particles due to shear strain is correlated with the extrusion temperature. Extrusions processed close to T_g showed significant porosity. All consolidates exhibit a glass transition at approximately the same temperature as the powder. On the other hand, the exothermic peak on the DSC curves is shifted to slightly lower temperatures for all extrusions. This shift is attributed to the formation of a small fraction of nanocrystalline islands and to the thermal-history effect. The decrease in T_x becomes more severe with increasing extrusion temperature. Extrusions processed at 440 °C show apparent crystallization, supported by the lack of a primary crystallization exothermic peak on the DSC trace as well as increased hardness and brittleness during Vickers microhardness testing. Shear banding is evident in hardness testing of the powder and all of the extrusions, except the sample processed at 440 °C. There was an increase in the consolidate hardness, depending on the extrusion temperature; however, there is not a direct correlation between the hardness values and the extrusion rate. Compression experiments demonstrated good consolidation and strength levels of 1500 to 1700 MPa, which are comparable to that of cast V106. In spite of some nanocrystallization and short-range-order formation upon processing, most of the fracture surfaces of the consolidates show shear banding and well-developed vein patterns, typical fracture characteristics of metallic glasses with good ductility. In some regions of the fracture surfaces, interparticle debonding is seen. The present results show that despite a relatively high oxygen content in the initial powder, ECAE is successful in consolidation of metallic glass powder in the supercooled liquid region.

REFERENCES

1. W.L. Johnson: *Materials Research Society Symposia Proc.,* Materials Research Society, Philadelphia, PA, 1999, vol. 554, p. 311.
2. W.L. Johnson: *JOM,* 2002, vol. 54 (3), p. 40.
3. H.A. Bruck, A.J. Rosakis, and W.L. Johnson: *J. Mater. Res.,* 1996, vol. 11, p. 503.
4. D.J. Sordelet, E. Rozhkova, P. Huang, P.B. Wheelock, M.F. Besser, M.J. Kramer, M. Calvo-Dahlborg, and U. Dahlborg: *J. Mater. Res.,* 2002, vol. 17, p. 186.
5. H. Kato, Y. Kawamura, and A. Inoue: *Mater. Trans. JIM,* 1996, vol. 37, p. 70.
6. Y. Kawamura, H. Kato, A. Inoue, and T. Masumoto: *Int. J. Powder Metall.,* 1997, vol. 33 (2), p. 50.
7. J. Robertson, J.-T. Im, I. Karaman, K.T. Hartwig, and I.E. Anderson: *J. Non-Crystalline Solids,* 2003, vol. 317, pp. 144-51.
8. Humberto Zapata: Master's Thesis, Texas A&M University, College Station, TX, 1998.
9. K.T. Hartwig, H. Zapata, A. Parasiris, and S. Mathaudhu: *Proc. Powder Materials: Current Research and Industrial Practices Symp.,* F.D.S. Marquis, N. Thadhani, and E.V. Barrera, eds., TMS, Warrendale, PA, 2001, pp. 211-21.
10. A. Parasiris, K.T. Hartwig, and M.N. Srinivasan: *Scripta Mater.*, 2000, vol. 42, p. 875.
11. K.T. Hartwig, G. Chase, and J. Belan: *Applied Superconductivity*, IEEE Trans., 2003, vol. 13, No. 2, p. 3548.
12. Liquid Metal Technologies Vitreloy 106 Data Sheet, Lake Forest, CA.
13. H. Choi-Yim, R.D. Conner, F. Szuecs, W.L. Johnson, *Acta Mater.,* 2002, vol. 50, p. 2737.
14. A. Inoue: *Mater. Sci. Foundations 6,* Trans Tech Publications, Aedermannsdorf, Switzerland, 1999.
15. A. Inoue: *Intermetallics,* 2000, vol. 8, pp. 455-68.
16. Y. Kawamura and A. Inoue: *Appl. Phys. Lett.,* 2000, vol. 77, p. 1114.
17. J.M. Pelletier, B. Van de Moortele, and I.R. Lu: *Science of Metastable and Nanocrystalline Alloys: Structure, Properties and Modeling,* Proc. 22nd, Risø Int. Symp. on Materials Science, A.R. Dinesen, M. Eldrup, D. Juul Jensen, S. Linderoth, T.B. Pedersen, and N.H. Pryds, eds., Risø National Laboratory, Roskilde, Denmark, 2001.